https://doi.org/10.52131/jmps.2020.0102.0009

Journal of Materials and Physical Sciences

Volume 1, Number 2, 2020, Pages 87 - 97

Journal Homepage:
https://journals.internationalrasd.org/index.php/jmps

JOURNAL OF MATERIALS AND PHYSICAL SCIENCES
INTERNATIONAL RESEARCH ASSOCIATION FOR SUSTAINABLE DEVELOPMENT

Magnesium Ferrite/Polyvinyl Alcohol (PVA) Nanocomposites: Fabrication and Characterization

Gulfam Nasar[1*], Muhammad Ishfaq[2], Fawad Ahmad[3], Shahbaz Nazir[4], Faseeh ur Raheem[5]

[1] Department of Chemistry, Balochistan University of Information Technology, Engineering and Management Sciences, Quetta 87300, Pakistan
[2] Punjab Higher Education Department, Govt. Graduate College Chishtian, Bahawalnagar, Pakistan
[3] Department of Chemistry, University of Wah, Quaid Avenue, Wah Cantt 47040 Pakistan
[4] Punjab Higher Education Department, Govt. Graduate College Ravi Road Shahdara, Lahore, Pakistan
[5] Institute of Physics, The Islamia University of Bahawalpur, Bahawalpur 63100, Pakistan

ARTICLE INFO

Article History:
Received: October 08, 2020
Revised: November 17, 2020
Accepted: December 19, 2020
Available Online: December 31, 2020

Keywords:
Spinel Ferrites
PVA Composites
XRD
FTIR
Dielectric Properties
Current-Voltage Measurements

ABSTRACT

Terbium doped magnesium spinel ferrites ($Mg_{1-x}Tb_xFe_2O_4$) with composition x=0.12, 0.14, 0.16, 0.18 were synthesized via micro-emulsion method followed by synthesis of PVA/$Mg_{1-x}Tb_xFe_2O_4$ composites using in-situ polymerization technique. The structural properties were evaluated using X-ray diffraction (XRD) and Fourier transform infra-red spectroscopy (FTIR). XRD analysis confirmed the construction of spinel lattice of terbium ferrite whereas FTIR revealed the interactions between ferrite nanoparticles and polyvinyl alcohol matrix. The XRD and FTIR results quite matched with the reported literature. The dielectric and resistivity analyses were performed by determining dielectric parameters and current-voltage measurements. The values of dielectric constant, dielectric loss and tan δ were found to be inversely proportional to the frequency under the ambient electric field at room temperature but became constant at higher frequency values. The lower values of dielectric constant of terbium incorporated magnesium ferrite polymer composites ($MgFe_2O_4$/PVA) are attributed to hindrance in 'electron exchange mechanism' created by lockup between iron and terbium ions. The resistivity values of all the composites were found from $2.5x10^9$ Ωcm to $18.8x10^9$ Ωcm which showed a non- linear behavior.

*Corresponding Author's Email: gulfamnasar@gmail.com

1. Introduction

Nanotechnology has exposed itself as the technology of miniaturization with an aim of making inexpensive, lighter and smarter goods having smaller sizes. Nano ferrite particles (having size less than 100 nm) have become much important during the last few decades and are considered as an effective link that bridges bulk substances and atomic or molecular materials(Abdelwahab & Shukry, 2015). Soft ferrites possess cubic spinel structure that is derived from $MgAl_2O_4$,(Reddy & Yun, 2016)whose structure was interpreted by Bragg. The general formula of magnetic spinels is MFe_2O_4 where M is a divalent transition element such as Mn, Fe, Co, Ni, Cu and Cd (Al-Ghamdi, Al-Hazmi, Memesh, Shokr, & Bronstein, 2017). All the ferrites contain iron oxide as the main constituent in their structures. The metal ions like Ni^{2+}, Co^{2+} and Mn^{2+} may also be used to offer the unpaired electron spins. The magnetic moment may also be disturbed by the incorporation of some non-paramagnetic ions such as Mg^{2+} or Zn^{2+} or monovalent Li, causing the variation in concentration of Fe^{3+} ions on the crystal lattice points. The spinel ferrites have received a lot of reputation. They have shown advantages of high saturation magnetization, high

electrical resistivity, high magnetic loss and low eddy current losses (Wang, Huang, Wang, He, & Chen, 2012). Generally the ferrite materials are cheap, stable and possess numerous applications related to technological and industrial fields(Davachi et al., 2016). They are used as microwave absorbers such as gas sensors(Balgis, Iskandar, Ogi, Purwanto, & Okuyama, 2011), isolators, gyrators, phase shifters, radio wave circuits, electronic equipment(Nasar et al., 2016), electrode materials, microwave dark rooms and protection, magneto-optical storage media manufacturing phenomena, optics and conducting adhesive materials, high density digital recording discs, spintronics(Mohamed, Rashad, Haraz, & Sigmund, 2010), noise filters(Chitra, Muthusamy, Dineshkumar, Jayaprakash, & Chandrasekar, 2015), hyperthermia(Jaberolansar, Kameli, Ahmadvand, & Salamati, 2016) high performance engineering materials and compact power supplies (Xiao, Liu, & Fu, 2006).

Material scientists have been making efforts to improve the properties of the nanofibers. It has been reported that sintering temperature and variation of different metal ions (dopants) especially of lanthanide series are observed to improve the electrical and magnetic properties of ferrite material effectively. The special emphasis on rare earth elements is due to their 4f unpaired electrons screened by $5s^2$ $5p^6$ electrons and strong spin –orbit coupling of the angular momentum which are not affected by the potential field of nearby ions and which can originate magnetic anisotropy owing to their orbital shape(Sun et al., 2015). Ferrites can be synthesized either by dry or wet method. The wet chemical routes include a vairiety of the processes comprising micro-emulsion, sol-gel, mechanochemical, hydrothermal, sol-spray drying, sonochemical, solvothermal, coprecipitation processes etc. (Naz, Durrani, Mehmood, & Nadeem, 2014). Rapidly developing field of polymer based nanocomposites has created a lot of inspiration for researchers during the recent years. Nanocomposites are known to possess multi-range systems as 1D, 2D, 3D and amorphous materials composed of diverse constituents at the nm size(Khairy & Gouda, 2015). They have various useful utilizations in electro-optical integrated instruments, energy storage devices (Gairola et al., 2010).

The efficiency of nanoferrite particles can be improved by incorporating them in polymer matrix owing to high surface area to volume ratio. Polymer nanocomposites are used in packaging materials, refractory materials(Chitra, Muthusamy, & Jayaprakash, 2015), high frequency multilayer chip inductors, transducers(Chen et al., 2016), optical integrated circuits, medical instruments, drug delivery from compartmented nanotubes, immobilization of biological objects like proteins, tissue engineering, fire retardants, adhesives, consumer goods etc.(Song, Shen, Liu, & Xiang, 2011).

Polymers used as matrix in magnetic nanocompoistes are commonly categorized in a number of classes such as neutral, charged, hydrophilic, homopolymers, co-polymers etc.(Fang & Zhang, 2009). Poly vinyl alcohol (PVA) is a synthetic polymer with poor electrical conductivity. It is commonly used owing to its diverse properties; such as solubility in water, excellent durability, moisture barrier film behavior,(Hmar, Majumder, & Mondal, 2016) semi-crystallinity, non-toxicity, better flexibility, highly transparent feature and emulsifying, biocompatibility, adhesion, biodegradability, very fine film making abilities etc. It is easily available and easy to handle(Kashyap, Pratihar, & Behera, 2016). A number of techniques have been reported fo synthesis of polymer nanocompoistes such as in-situ polymerization, electrochemical, micro-emulsion, electro spinning etc.(Bose et al., 2010). Rashidi, S. and A. Ataie used a two-step mechanical milling technique to manufacture the advanced functional magnetic nanocomposites having polyvinyl alcohol and cobalt ferrite ($PVA/CoFe_2O_4$) as main constituents. They reported the effects of milling time and polymer fraction. They prepared the spherical single-phase cobalt ferrite of about 20 ± 4 nm and embedded them in PVA by rigorous milling. The synthesized nanomaterial showed decreasing trend in magnetic properties like saturation magnetization, coercivity and anisotropy constant values(S Rashidi & A Ataie, 2016).

We report an innovative, cheaper, facile and economical method of synthesizing $PVA/Mg_{1-x}Tb_xFe_2O_4$ nanocomposites using in-situ polymerization technique via ultra-sonication. The effect of Tb substitution with Mg has been studied in terms of morphology, electrical and DC conductivity of $PVA/Mg_{1-x}Tb_xFe_2O_4$ nanocomposites.

2. Experimental Procedure

2.1. Chemicals Used

The following chemicals were used for the synthesis of PVA/$Mg_{1-x}Tb_xFe_2O_4$ nanocomposite materials. Magnesium chloride, $MgCl_2.4H_2O$ (Sigma-Aldrich, 98%), Terbium chloride, $TbCl_3.6H_2O$ (Sigma-Aldrich, 99.9%), Iron chloride, $FeCl_3.6H_2O$ (Merck, 99%), Aqueous NH_3 (BDH, 35%), Polyvinyl alcohol (PVA), Arcos, England (mol. wt= 70,000 g mol^{-1}), CTAB, Cetyltrimethyl ammonium bromide, $(C_{16}H_{33})$ N $(CH_3)_3Br$, (Amresco, 98%), Sodium carbonate, $NaCO_3$, (Riedel-deHaen) and De-ionized water. All the chemicals were used as received without further purification.

2.2. Synthesis of $Mg_{1-x}Tb_xFe_2O_4$ Nanoparticles

Terbium doped $Mg_{1-x}Tb_xFe_2O_4$ nanoferrites with composition x=0.12, 0.14, 0.16, 0.18 were prepared via wet chemical route i.e. micro-emulsion method. The stoichiometric amounts of reagents were dissolved in de-ionized water. The solutions were stirred using magnetic stirrer at 50-60C°. and "CTAB" was added drop-wise to the stirring solutions. The pH 10-11 was attained by adding 2M aqueous solution of NH_3 while the stirring was continued for further 5-6 hours. The precipitates were washed with de-ionized water several times to obtain pH 7, followed by drying in oven at 100 C°. The prepared samples were annealed at 700 C° for 7 hours in Muffle furnace at heating rate of 5 C° /min. The synthesized $Mg_{1-x}Tb_xFe_2O_4$ nanoferrites were ground finely using ultraclean pestle and mortar (Khan, Islam, Ishaque, & Rahman, 2012).

2.3. Synthesis of PVA/$Mg_{1-x}Tb_xFe_2O_4$ Nanocomposites

The PVA/$Mg_{1-x}Tb_xFe_2O_4$ nanocomposites were synthesized via ultra-sonication. Five compositions of nanocomposites were prepared with 1.5 g of PVA in each composition. Likewise a blank PVA film was prepared for comparison. Mg ferrite was added in each composition as x (x = 0.12, 0.14, 0.16, 0.18). The solution of polymer was prepared by stirring and at 70-80 C° using de-ionized water as solvent. Finely ground $Mg_{1-x}Tb_xFe_2O_4$ nanoparticles were suspended via sonication in de-ionized water. Both the solutions were mixed and sonicated at 60-70 C° for two hours. The resulting solution was poured in petri dish and dried at room temperature to get thin film of PVA/$Mg_{1-x}Tb_xFe_2O_4$ nanocomposites.

3. Results and Discussion

3.1. X-Ray Diffraction (XRD)

XRD diffraction of pure PVA and the PVA/$Mg_{1-x}Tb_xFe_2O_4$ nanocomposites films was carried out by BRUKER AXS GmbH, Ostliche Rheinbruckenstr, 76187 Karlsruhe Germany/Alemania/Allemagne using Cu Kα radiation of wavelength λ=1.54060Å filtered with "Ni". XRD profile of pure PVA and PVA/$Mg_{1-x}Tb_xFe_2O_4$ nanocomposites (x=0.12 to 0.18) is shown in Fig.1. The results show the main peak at 2θ=19.8° which corresponds to (101) crystal plane of pure PVA indicating its semi-crystalline nature as reported by Mohanapriya, M.K., et al(Mohanapriya, Deshmukh, Ahamed, Chidambaram, & Khadheer Pasha, 2016). Some other diffraction peaks indexed as (220), (311), (400), (422), (511) and (440) at 2θ° values, 30.1, 35.39, 42.97, 53.50, 57.09, 62.62 respectively. The most dominant peak appeared at 35.39° corresponding to crystal plane (311) which is the confirmation of single phase FCC spinel structure of $MgFe_2O_4$.These observed XRD profiles of the composites have a perfect matching with those of standard diffraction profiles of JCPDS card # 36-0398. All the above mentioned diffraction profiles have already been reported and revealed the FCC single spinel structure of the resulting PVA/$Mg_{1-x}Tb_xFe_2O_4$ nanocomposites. The prominent peak relating to (311) plane is present in all the synthesized nanocomposites. The intensities of two more planes i.e. (220) and (400) are also much sensitive to cations on tetrahedral (A sites) and octahedral (B sites) sites respectively. Observations through experiments have demonstrated that Mg^{2+} has a strong preference to occupy B-sites and partially occupy A-sites.

The ionic radii of Mg^{2+} and Tb^{3+} are 0.66Å and 0.93 Å respectively. The observed intensities of the above mentioned peaks decline remarkably by the substitution of Tb^{3+} by Mg^{2+} ions. The intensity of peak corresponding to plane (400) is relatively more decreased because of this substitution which largely depends upon the bigger size of Tb^{3+} ions. The various lattice parameters are calculated using the following relationships:

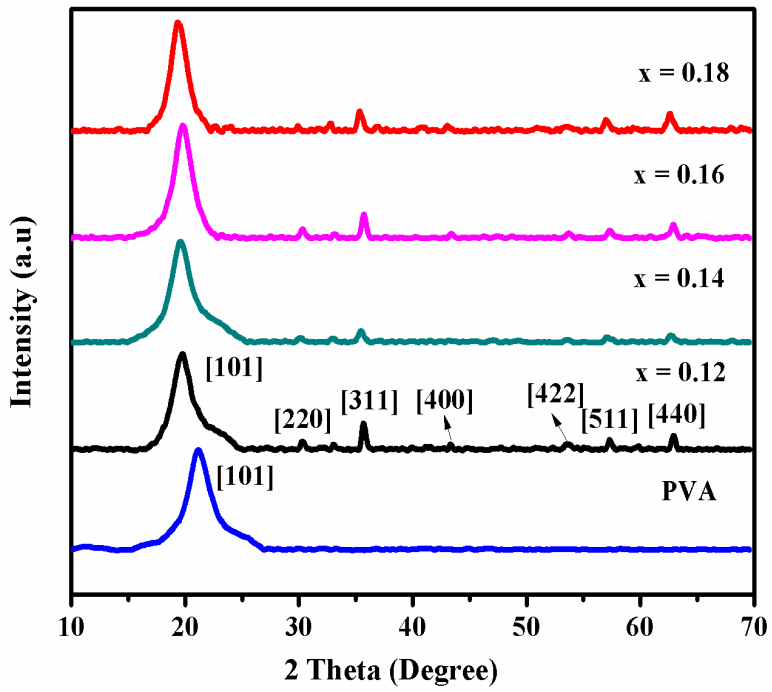

Figure 1: XRD pattern of uncoated PVA and PVA/$Mg_{1-x}Tb_x$ Fe_2O_4 nanocomposites

Crystalline size (D) = $\frac{0.9\lambda}{\beta\cos\theta}$ (Debye-Scherer's formula) (1)

Where β is the average full width at half maxima (FWHM), θ is the Bragg's angle and λ is the X-ray wavelength.

X-ray density ($\rho_{x\text{-ray}}$) = $\frac{8M}{N_A V}$ (2)

Where M is the mass of the composite, N_A is the Avogadro's number and V is the volume of the composite film.

Bulk density (ρ_{bulk}) = $\frac{m}{v}$ (3)

Where 'm' is mass and 'v' is the volume of thin film.

Porosity (P) = $1-\frac{\rho_{bulk}}{\rho_{x-ray}}$ (4)

Table 1:
Different values of lattice parameters of PVA/$Mg_{1-x}Tb_xFe_2O_4$ (x=0.12, 0.14, 0.16, 0.18)

Sample Composition	Lattice Constant(a) Å	Cell Volume $(Å)^3$	X-ray Density (gcm^{-3})	Bulk Density (gcm^{-3})	Porosity (P)	Crystallite Size (nm)
X=0.12	8.39	590.59	4.86	2.58	47	30.96
X=0.14	8.38	588.48	4.94	2.89	41	23.76
X=0.16	8.36	584.28	5.04	2.49	50	31.06
X=0.18	8.35	582.18	5.12	2.61	49	25.36

3.2. Fourier-Transform Infra-Red Spectroscopy (FTIR)

The Fourier Transform Infrared Spectroscopy of pure PVA and nanocomposite films was carried out using MIDAC M 2000 with wavenumber range 600-4000 cm^{-1} in transmittance mode. The obtained spectrum has the set of absorption bands whose intensity and frequency offer facts about structure and bonding within the molecule (Kubicki et al., 2012). FTIR spectra of pure PVA and nanocomposites are shown in Fig 2. In case of pure PVA, the main absorption peaks are found at 3295 cm^{-1}, due to O-H stretching (responsible for H-bonding), 2927cm^{-1},is due to C-H stretching,1729 cm^{-1} and1567 cm^{-1} correspond to C=O stretching and C=O asymmetric stretching and near 1419 cm^{-1} ,due to C-H bending vibrations. The absorption peaks located near 1148 cm^{-1} and 1090 cm^{-1} reveal the stretching mode of Fe-O-Fe groups (S. Rashidi & A. Ataie, 2016). The presence of all these peaks confirms the existence and incorporation of pure PVA matrix in all the resulting PVA/$Mg_{1-x}Tb_xFe_2O_4$ nanocomposites.

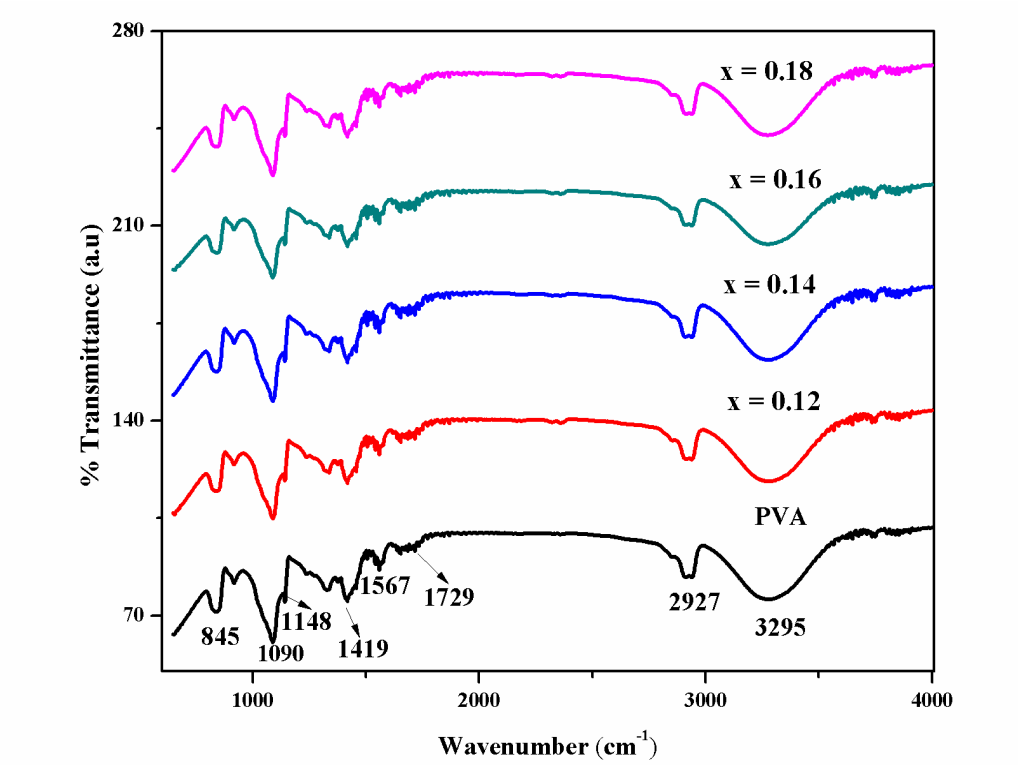

Figure 2: FTIR spectra of pure PVA and PVA/$Mg_{1-x}Tb_x$ Fe_2O_4 nanocomposites

3.3. Dielectric Measurements

4287 A RF LCR meter was used to determine the dielectric measurements in the frequency range of 0.0-3GHz at room temperature. These measurements are much important for engineers and material scientists to design electronic devices. The thin films of pure PVA matrix and the fabricated PVA/$Mg_{1-x}Tb_xFe_2O_4$ nanocomposites (x=0.12, 0.14, 0.16, 0.18) were analyzed. Dielectric constant , which is a measure of extent of polarization of a material, depends upon the structure of the materials, composition and the method of preparation involved (Lodhi et al., 2014).

The dielectric parameters like dielectric constant (ε'), dielectric loss and dielectric tangent loss (tanδ) were measured. It is notable that all the dielectric parameters are function of the applied alternating current field in the above mentioned frequency range. The dielectric constant was calculated with the help of equation 5 (Khan et al., 2012).

$$\varepsilon' = \frac{cd}{\varepsilon_0 A} \qquad (5)$$

Where d is the thickness of the material, c is the capacitance of the material, $\varepsilon_\circ$ is the permittivity of free space and A is the cross-sectional area of the flat surface of the material in m^2. The variation of dielectric constant (ε') as function of frequency has been shown in Figure 3.

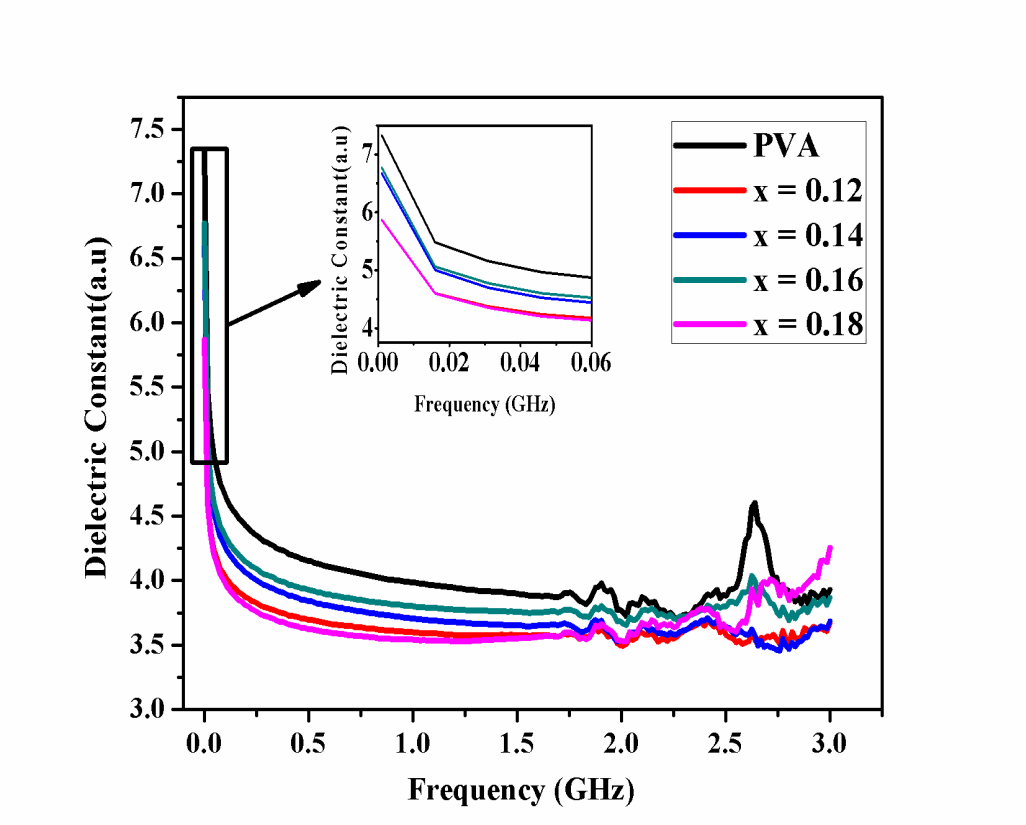

Figure 3: The variation of dielectric constant with frequency of pure PVA and PVA/$Mg_{1-x}Tb_x$ Fe_2O_4 nanocomposites.

The values of dielectric constant show a decreasing trend with the successive exchange of Tb^{3+} ions. In the spinel structure of magnesium ferrite ($MgFe_2O_4$), there are two sites namely A-sites (tetrahedral) and B-sites (octahedral). It is well-known that most of the Mg ions occupy on B-sites whereas Fe ions occupy on both A and B-sites (Hemeda, Said, & Barakat, 2001). Dielectric constant values gradually decrease with substitution of terbium ions with magnesium ions. This is attributed to the increase of Tb ions substitution on B-sites replaces some Mg ions (number of Mg ions on B-sites decreased) which leads to the reduction in population of Fe^{2+} ions (Mg^{2+} + Fe^{3+} ↔ Mg^{3+} + Fe^{2+}) on B-sites. As a result, the electron exchange interaction happening at B-sites between the Fe^{3+} ions and Fe^{2+} ions hindered due to the existence of Tb ions on B-sites, so the hopping length of conduction electrons rises. Thus, description justifies the decrease in the dielectric constant values with the growing concentration of Tb ions.

Initially, the dielectric constants for pure PVA and all the fabricated samples decrease more rapidly with an increase in frequency (low region) but in the high frequency region, the value drops down to minimum and becomes almost constant. At lower frequencies, the higher values of dielectric constant are attributed to some polarizations like space charge, dipolar, ionic and electronic types (Choudhury, Rodríguez, Bhattacharya, Katiyar, & Rinaldi, 2007). This behavior can be explained on the basis of the Maxwell Wagner model which is in agreement with Koops phenomenological theory (Costa, Tortella, Morelli, & Kiminami, 2003).

An additional interfacial space charge polarization plays a prominent role in these types of heterogeneous composites and that increases the dielectric constant. The interfacial polarization gives response very slowly to the external field; therefore, it governs largely in the low frequency region and has no significant influence in the high frequency region. Dielectric constant values become constant at higher frequency values attributed to

the fact that space charge carriers(dipoles) of the composite material do not find much time to re-orient themselves (lagging off polarization) in the direction of the applied electric field (Ali et al., 2014).

The dielectric loss measures the loss of electrical energy from the applied electric field into the samples at different frequencies. The dielectric tangent loss (tanδ) was calculated using the relation 6 (Mohamed et al., 2010).

$$\text{Tan}\delta = \frac{\varepsilon''}{\varepsilon'} \qquad (6)$$

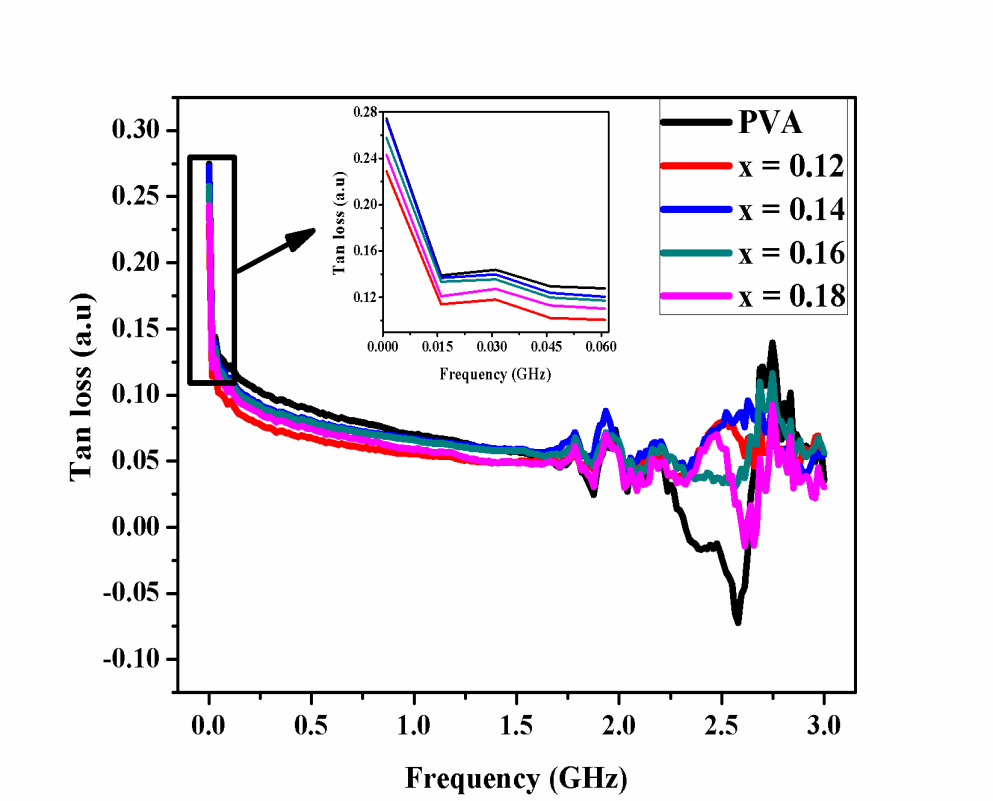

Figure 4: The variation of dielectric tangent loss with frequency of pure PVA and PVA/$Mg_{1-x}Tb_x$ Fe_2O_4 nanocomposites

Where tanδ is the loss angle, ε'' is the imaginary part of the dielectric constant and is the total amount of the absorbed energy by the material used from the alternating field ε' is the real part of the dielectric constant. The graph of dielectric loss tangent versus frequency is depicted in figure 4. The variation of dielectric loss with frequency in the applied electric field is quite similar to the real part of the dielectric constant (ε') and depends upon conduction mechanism, composition of material, annealing temperature, synthesis technique, crystalline size etc. Electron hopping and defect dipoles are major contributors in this regards. Electron hopping is responsible only in low frequency region and it becomes ineffective at higher frequency values, hence dielectric loss decreases. The dielectric loss also shows the peaking behavior i.e. resonance peaks have been observed at higher frequency values as cleared from the Fig. 4. At high frequency, it is the jumping frequency of Fe^{2+} and Fe^{3+} which becomes equal to the frequency of applied electric field. This peaking behavior is because of Debye-type relaxation. The loss factors of these samples have been observed to decrease with the increase in frequency as shown in figure 5. It has been demonstrated that ionic radius of doping species (Tb^{3+}) is directly proportional to the polarization and the frequency of the applied electric field vary to the inverse of polarization**.** As the concentration of Tb^{3+} increases, the grain size also increases but grain boundaries per unit volume decrease which ultimately reduces the dielectric loss. All the Tb^{3+} substituted samples exhibit low values of loss factor as compared to the unsubstituted sample. In the high frequency region, the loss factor indicates very small values. (Khan et al., 2012).

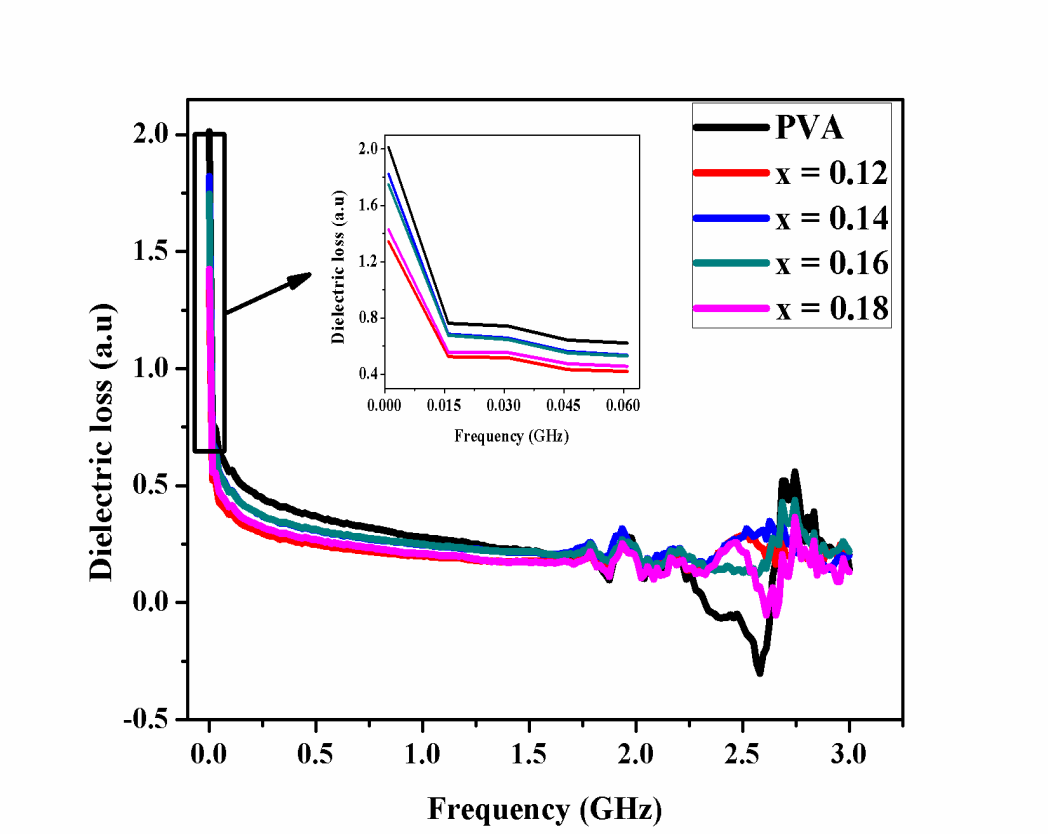

Figure 5: The variation of dielectric loss factor with frequency of pure PVA and PVA/$Mg_{1-x}Tb_x$ Fe_2O_4 nanocomposites

3.4. Current-Voltage Measurements (I-V)

The current–voltage specific (I–V) curve is a typical graphical relationship between the electric current passing through a substance and its corresponding voltage across that substance. The graph obtained through this procedure is helpful for electronic engineers to decide the fundamental behavior of the substance in the electric powered circuit (van der Bijl, 1919).

Current-voltage study of the synthesized PVA/$Mg_{1-x}Tb_xFe_2O_4$ nanocomposites (x=0.12, 0.14, 0.16, 0.18) was done using 6487 Pico Ammeter/Voltage source (Kiethely) at standard conditions. The voltage of the used apparatus was adjusted at -5 to 5 volts. The resulting I-V curves of pure PVA and PVA/$Mg_{1-x}Tb_xFe_2O_4$ nanocomposites (x=0.12, 0.14, 0.16, 0.18) as shown in Figure 6. To calculate the values of resistivity, the following formula was used.

$$\text{Resistivity} = \frac{RA}{L} \qquad (7)$$

Where L, A and R are taken as thickness, area and resistance of polymer composite films respectively as reported by Shahzad, M.A., et al(Shahzad, Warsi, Khan, Iqbal, & Asghar, 2015). The resistivity values obtained of all the composites are shown in the Table 4.2 having the range of $2.5x10^9$ Ωcm to $18.8x10^9$ Ωcm which showed a non- linear behavior. It was due to the substitution of Tb^{3+} in the base materials as reported by Rasheed, A., et al(Rasheed et al., 2016).

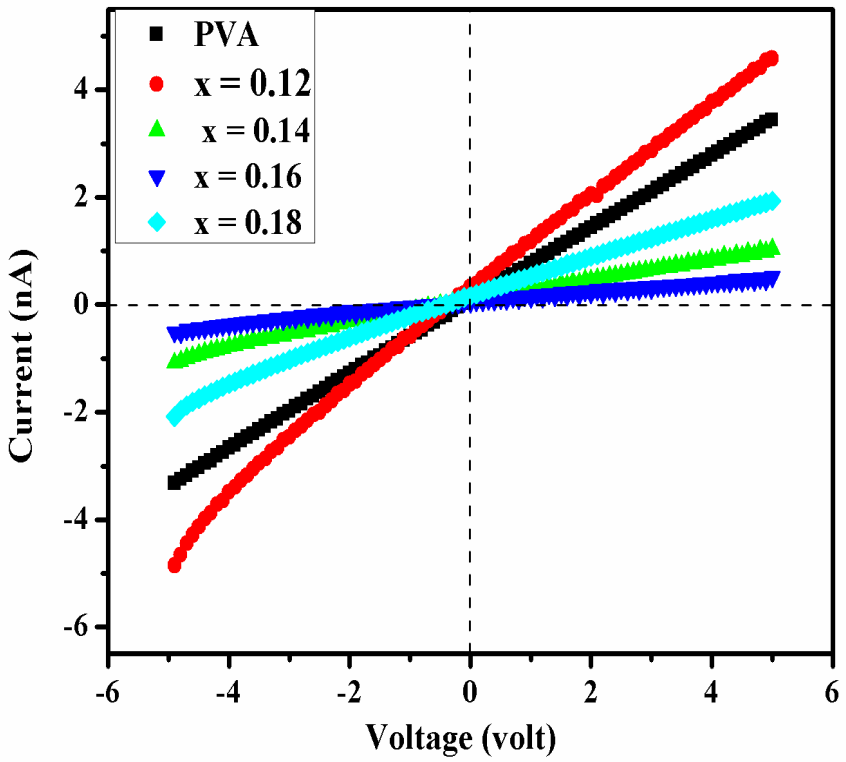

Figure 6: Current Voltage (I-V) Characteristics of pure PVA and PVA/$Mg_{1-x}Tb_x Fe_2O_4$ nanocomposites

Table 2
Resistivity values of pure PVA and PVA/$Mg_{1-x}Tb_xFe_2O_4$ nanocomposites (x=0.12, 0.14, 0.16, 0.18)

Sr. no	Composition	Resistivity (Ωcm)
1	PVA	2.5 X 10^9
2	$Mg_{0.88}Tb_{0.12}Fe_2O_4$	2.08 X 10^9
3	$Mg_{0.86}Tb_{0.14}Fe_2O_4$	8.5 X 10^9
4	$Mg_{0.84}Tb_{0.16}Fe_2O_4$	18.8 X 10^9
5	$Mg_{0.82}Tb_{0.18}Fe_2O_4$	4.47 X 10^9

4. Conclusion

Nanocrystalline magnesium ferrites with terbium substitution ($Mg_{1-x}Tb_xFe_2O_4$) having composition, x=0.12, 0.14, 0.16, 0.18 were successfully prepared followed by synthesis of PVA/$Mg_{1-x}Tb_xFe_2O_4$ nanocomposites employing a cheaper wet chemical method and solution casting technique respectively. The XRD and FTIR studies demonstrated the FCC single phase spinel structure. The interactions between nanoferrite particles and PVA matrix is also confirmed. The lattice constants and subsequently cell volume decreased with increasing Tb^{3+} content. The dielectric and I-V values were measured to elucidate the practical applications. The dielectric constants and dielectric loss (tanδ) for all the synthesized materials had an inverse relationship with the frequency in the applied electrical field. The dielectric parameters also showed an inverse behavior with resistivity.

References

Abdelwahab, N. A., & Shukry, N. (2015). Synthesis, characterization and antimicrobial properties of grafted sugarcane bagasse/silver nanocomposites. *Carbohydrate Polymers, 115*(0), 276-284. doi:http://dx.doi.org/10.1016/j.carbpol.2014.08.052

Al-Ghamdi, A. A., Al-Hazmi, F. S., Memesh, L. S., Shokr, F. S., & Bronstein, L. M. (2017). Effect of mechanochemical synthesis on the structure, magnetic and optical behavior

of Ni1−xZnxFe2O4 spinel ferrites. *Ceramics International, 43*(8), 6192-6200. doi:http://dx.doi.org/10.1016/j.ceramint.2017.02.017

Ali, R., Khan, M. A., Mahmood, A., Chughtai, A. H., Sultan, A., Shahid, M., . . . Warsi, M. F. (2014). Structural, magnetic and dielectric behavior of Mg1−xCaxNiyFe2−yO4 nano-ferrites synthesized by the micro-emulsion method. *Ceramics International, 40*(3), 3841-3846. doi:http://dx.doi.org/10.1016/j.ceramint.2013.08.024

Balgis, R., Iskandar, F., Ogi, T., Purwanto, A., & Okuyama, K. (2011). Synthesis of uniformly porous NiO/ZrO2 particles. *Materials Research Bulletin, 46*(5), 708-715. doi:http://dx.doi.org/10.1016/j.materresbull.2011.01.019

Bose, S., Kuila, T., Uddin, M. E., Kim, N. H., Lau, A. K., & Lee, J. H. (2010). In-situ synthesis and characterization of electrically conductive polypyrrole/graphene nanocomposites. *Polymer, 51*(25), 5921-5928.

Chen, F., Zhang, Z., Wang, X., Ouyang, J., Feng, Z., Su, Z., . . . Harris, V. G. (2016). Room temperature magnetoelectric effect of YFeO3–Y3Fe5O12 ferrite composites. *Journal of Alloys and Compounds*(656), 465-469.

Chitra, P., Muthusamy, A., Dineshkumar, S., Jayaprakash, R., & Chandrasekar, J. (2015). Temperature and frequency dependence on electrical properties of polyaniline/Ni(1−x)CoxFe2O4 nanocomposites. *Journal of Magnetism and Magnetic Materials, 384*, 204-212. doi:http://dx.doi.org/10.1016/j.jmmm.2015.02.040

Chitra, P., Muthusamy, A., & Jayaprakash, R. (2015). Structural, magnetic and dielectric properties of polyaniline/MnCoFe 2 O 4 nanocomposites. *Journal of Magnetism and Magnetic Materials, 396*, 113-120.

Choudhury, R. N. P., Rodríguez, C., Bhattacharya, P., Katiyar, R. S., & Rinaldi, C. (2007). Low-frequency dielectric dispersion and magnetic properties of La, Gd modified Pb(Fe1/2Ta1/2)O3 multiferroics. *Journal of Magnetism and Magnetic Materials, 313*(2), 253-260. doi:http://dx.doi.org/10.1016/j.jmmm.2007.01.005

Costa, A., Tortella, E., Morelli, M., & Kiminami, R. (2003). Synthesis, microstructure and magnetic properties of Ni–Zn ferrites. *Journal of Magnetism and Magnetic Materials, 256*(1), 174-182.

Davachi, S. M., Kaffashi, B., Torabinejad, B., Zamanian, A., Seyfi, J., & Hejazi, I. (2016). Investigating thermal, mechanical and rheological properties of novel antibacterial hybrid nanocomposites based on PLLA/triclosan/nano-hydroxyapatite. *Polymer, 90*, 232-241. doi:http://dx.doi.org/10.1016/j.polymer.2016.03.007

Fang, C., & Zhang, M. (2009). Multifunctional magnetic nanoparticles for medical imaging applications. *Journal of Materials Chemistry, 19*(35), 6258-6266.

Gairola, S., Verma, V., Kumar, L., Dar, M. A., Annapoorni, S., & Kotnala, R. (2010). Enhanced microwave absorption properties in polyaniline and nano-ferrite composite in X-band. *Synthetic Metals, 160*(21), 2315-2318.

Hemeda, O., Said, M., & Barakat, M. (2001). Spectral and transport phenomena in Ni ferrite-substituted Gd 2 O 3. *Journal of Magnetism and Magnetic Materials, 224*(2), 132-142.

Hmar, J., Majumder, T., & Mondal, S. (2016). Growth and characteristics of PbS/polyvinyl alcohol nanocomposites for flexible high dielectric thin film applications. *Thin Solid Films, 598*, 243-251.

Jaberolansar, E., Kameli, P., Ahmadvand, H., & Salamati, H. (2016). Synthesis and characterization of PVP-coated Co0. 3Zn0. 7Fe2O4 ferrite nanoparticles. *Journal of Magnetism and Magnetic Materials, 404*, 21-28.

Kashyap, S., Pratihar, S. K., & Behera, S. K. (2016). Strong and ductile graphene oxide reinforced PVA nanocomposites. *Journal of Alloys and Compounds*.

Khairy, M., & Gouda, M. (2015). Electrical and optical properties of nickel ferrite/polyaniline nanocomposite. *Journal of advanced research, 6*(4), 555-562.

Khan, M. A., Islam, M. U., Ishaque, M., & Rahman, I. Z. (2012). Magnetic and dielectric behavior of terbium substituted Mg1−xTbxFe2O4 ferrites. *Journal of Alloys and Compounds, 519*, 156-160. doi:https://doi.org/10.1016/j.jallcom.2011.12.159

Kubicki, J. D., Paul, K. W., Kabalan, L., Zhu, Q., Mrozik, M. K., Aryanpour, M., . . . Strongin, D. R. (2012). ATR–FTIR and Density Functional Theory Study of the Structures, Energetics, and Vibrational Spectra of Phosphate Adsorbed onto Goethite. *Langmuir, 28*(41), 14573-14587. doi:10.1021/la303111a

Lodhi, M. Y., Mahmood, K., Mahmood, A., Malik, H., Warsi, M. F., Shakir, I., . . . Khan, M. A. (2014). New Mg0.5CoxZn0.5−xFe2O4 nano-ferrites: Structural elucidation and electromagnetic behavior evaluation. *Current Applied Physics, 14*(5), 716-720. doi:http://dx.doi.org/10.1016/j.cap.2014.02.021

Mohamed, R., Rashad, M., Haraz, F., & Sigmund, W. (2010). Structure and magnetic properties of nanocrystalline cobalt ferrite powders synthesized using organic acid precursor method. *Journal of Magnetism and Magnetic Materials, 322*(14), 2058-2064.

Mohanapriya, M. K., Deshmukh, K., Ahamed, M. B., Chidambaram, K., & Khadheer Pasha, S. K. (2016). Influence of Cerium Oxide (CeO2) Nanoparticles on the Structural, Morphological, Mechanical and Dielectric Properties of PVA/PPy Blend Nanocomposites. *Materials Today: Proceedings, 3*(6), 1864-1873. doi:http://dx.doi.org/10.1016/j.matpr.2016.04.086

Nasar, G., Khan, M. A., Warsi, M. F., Shahid, M., Khalil, U., & Khan, M. S. (2016). Structural and electromechanical behavior evaluation of polymer-copper nanocomposites. *Macromolecular Research, 24*(4), 309-313. doi:10.1007/s13233-016-4043-3

Naz, S., Durrani, S. K., Mehmood, M., & Nadeem, M. (2014). Hydrothermal synthesis, structural and impedance studies of nanocrystalline zinc chromite spinel oxide material. *Journal of Saudi Chemical Society*.

Rasheed, A., Mahmood, M., Ali, U., Shahid, M., Shakir, I., Haider, S., . . . Warsi, M. F. (2016). Zr x Co 0.8− x Ni 0.2− x Fe 2 O 4-graphene nanocomposite for enhanced structural, dielectric and visible light photocatalytic applications. *Ceramics International, 42*(14), 15747-15755.

Rashidi, S., & Ataie, A. (2016). Structural and magnetic characteristics of PVA/CoFe2O4 nano-composites prepared via mechanical alloying method. *Materials Research Bulletin, 80*, 321-328. doi:http://dx.doi.org/10.1016/j.materresbull.2016.04.021

Rashidi, S., & Ataie, A. (2016). Structural and magnetic characteristics of PVA/CoFe 2 O 4 nano-composites prepared via mechanical alloying method. *Materials Research Bulletin, 80*, 321-328.

Reddy, D. H. K., & Yun, Y.-S. (2016). Spinel ferrite magnetic adsorbents: Alternative future materials for water purification? *Coordination Chemistry Reviews, 315*, 90-111. doi:http://dx.doi.org/10.1016/j.ccr.2016.01.012

Shahzad, M. A., Warsi, M. F., Khan, M. A., Iqbal, F., & Asghar, M. (2015). New Nd-doped lead zirconate Pb1−1.5xNdxZrO3 nanocrystals: Fabrication via wet chemical route for electrical and dielectric parameters evaluation. *Journal of Alloys and Compounds, 647*, 693-698. doi:http://dx.doi.org/10.1016/j.jallcom.2015.06.096

Song, F., Shen, X., Liu, M., & Xiang, J. (2011). Preparation and magnetic properties of SrFe 12 O 19/Ni 0.5 Zn 0.5 Fe 2 O 4 nanocomposite ferrite microfibers via sol–gel process. *Materials Chemistry and Physics, 126*(3), 791-796.

Sun, K., Wang, J., Yang, Y., Li, Y., Yu, Z., Lan, Z., . . . Wu, C. (2015). Influence of Ta2O5–Co2O3 co-doping on the magnetic property of NiMgCuZn ferrites. *Physica B: Condensed Matter, 476*, 122-128. doi:http://dx.doi.org/10.1016/j.physb.2015.03.023

van der Bijl, H. J. (1919). Theory and Operating Characteristics of the Thermionic Amplifier. *Radio Engineers, Proceedings of the Institute of, 7*(2), 97-128. doi:10.1109/jrproc.1919.217425

Wang, Y., Huang, Y., Wang, Q., He, Q., & Chen, L. (2012). Preparation and electromagnetic properties of Polyaniline(polypyrrole)-BaFe12O19/Ni0.8Zn0.2Fe2O4 ferrite nanocomposites. *Applied Surface Science, 259*, 486-493. doi:http://dx.doi.org/10.1016/j.apsusc.2012.07.072

Xiao, H.-M., Liu, X.-M., & Fu, S.-Y. (2006). Synthesis, magnetic and microwave absorbing properties of core-shell structured MnFe 2 O 4/TiO 2 nanocomposites. *Composites Science and Technology, 66*(13), 2003-2008.